

## GAMMA-RAY LIGHT CURVES AND SPECTRA OF MODELS FOR TYPE Ia SUPERNOVAE

P. HÖFLICH,<sup>1</sup> A. KHOKHLOV,<sup>2</sup> & E. MÜLLER<sup>3</sup><sup>1</sup>Institute for Astrophysics, University of Munich, Scheinerstraße 1, 8 München, Germany, <sup>2</sup>University of Texas, Austin, TX 78712-1083,<sup>3</sup>MPI für Astrophysik, Karl-Schwarzschild-Strasse 1, W-8046 Garching, Germany

Received 1993 May 4; accepted 1993 July 30

## ABSTRACT

Based on detailed Monte Carlo calculations, we present  $\gamma$ -ray energy deposition functions,  $\gamma$ -ray light curves, and  $\gamma$ -ray spectra for a large set of theoretical models of Type Ia supernovae including “classical” detonation and deflagration, delayed detonation, explosions of low mass white dwarfs, and tamped detonation scenarios.

Our computations show that models for Type Ia supernovae can be discriminated and the absolute amount of  $^{56}\text{Ni}$  synthesized in the event can be determined on the basis of the  $\gamma$ -ray light curves and spectra if  $\gamma$ -ray measurements are combined with observations at other wavelengths, e.g., in the optical band. We discuss at which times  $\gamma$ -ray observations are most suitable and needed from the theoretical point of view.

The implication of the upper limit in the  $\gamma$ -ray flux by *CGRO* experiment for our understanding of SN 1991T is discussed. We find that this limit is consistent with both the optical light curve and the implied distance (12.5 Mpc), i.e., several models can be ruled out by the  $\gamma$ -ray observations.

*Subject headings:* gamma rays: theory — supernovae: general — supernovae: individual (SN 1991T)

## 1. INTRODUCTION

Nowadays it is widely accepted that Type Ia supernovae (SN Ia's) are thermonuclear explosions of degenerate stellar configurations but the details are not yet clear. In a first group of scenarios the explosion occurs in massive carbon-oxygen white dwarfs close to the Chandrasekhar mass and the explosion is triggered by compressional heat due to the accretion through the Roche-lobe overflow from a companion star (Nomoto, Sugimoto, & Neo 1976). The second group of configurations are the outcome of the so-called merger scenario (e.g., Webbink 1984; Iben & Tutukov 1984).

While both the progenitor evolution and the mode of explosion of SN Ia's are still a matter of controversial debates it is commonly accepted that radioactive  $^{56}\text{Ni}$  synthesized in the event and its likewise radioactive decay product  $^{56}\text{Co}$  power the maximum and post-maximum optical light curve (Colgate & McKee 1969), i.e., the  $\gamma$ -lines from SN Ia should provide for a good diagnostical tool to reduce the uncertainties from the models (Clayton, Colgate, & Fishman 1969).

In the following we present the results of detailed Monte Carlo calculations of the  $\gamma$ -ray signature of theoretical SN Ia models based on the detonation, deflagration and delayed detonation of carbon-oxygen WDs (see Table 1). In addition, we have analyzed two further kinds of SN Ia models, which are variants of the delayed detonation model and the detonation model: (i) a delayed detonation giving rise to a large-scale pulsation of the white dwarf, and (ii) detonations of low mass white dwarfs surrounded by a low density envelope crudely resembling a merger configuration. Finally, our results are applied to SN 1991T and the advantages of combining model calculations both of the  $\gamma$  and optical wavelength range are demonstrated. For more details see Khokhlov (1991), Höflich, Müller, & Khokhlov (1992), Khokhlov, Müller & Höflich (1993), and Höflich, Khokhlov & Müller (1993).

## 2. SOME GENERAL RESULTS

Type Ia supernova models can be discriminated and the absolute amount of  $^{56}\text{Ni}$  synthesized in the event can be obtained on the basis of the  $\gamma$ -ray light curves and spectra (Figs. 1–2). We find that the appearance of the  $\gamma$ -rays are mainly determined by the  $^{56}\text{Ni}$ -distribution and the expansion rate of the ejecta. In particular, the rise time of the LC is very sensitive to these characteristics (see Fig. 2). Line ratios provide important information about the  $^{56}\text{Ni}$ -distribution in the outer layers of ejecta. Measurements of line profiles can also be used to determine the size of the central hole in the distribution of  $^{56}\text{Ni}$  produced by neutronization occurring in high-density progenitors. The central hole causes profiles with a boxlike shape at late times (see Fig. 1). The size of this central region with little  $^{56}\text{Ni}$  can be changed, e.g., by mixing processes which in turn changes the  $\gamma$  line profiles from box like into triangle like shapes (DF1  $\Rightarrow$  DF1MIX). Similar profiles are also produced in low density detonations because of the lack of strong neutronization processes (Table 1 and Fig. 1). However, the two reasons (small neutronisation and mixing processes) can well be distinguished on the basis of the early  $\gamma$ -ray light curve (compare DF1MIX and DET2, Fig. 2) if Type Ia supernova are observed at least at two different epochs, one of which has to be within about two weeks after the explosion.

## 3. SN 1991T

SN Ia's are long known to be strong sources of  $\gamma$ -rays but, for the first time, the chance for measurements came up with the launch of *CGRO* in accord to the discovery of SN 1991T in the SB galaxy NGC 4527 on 1991 April 13. It had been predicted (e.g., Müller, Höflich, & Khokhlov 1991) that a SN Ia can be observed with *CGRO* if (i) a supernova explodes within a distance of a few Mpc's during the active life of the satellite, and if

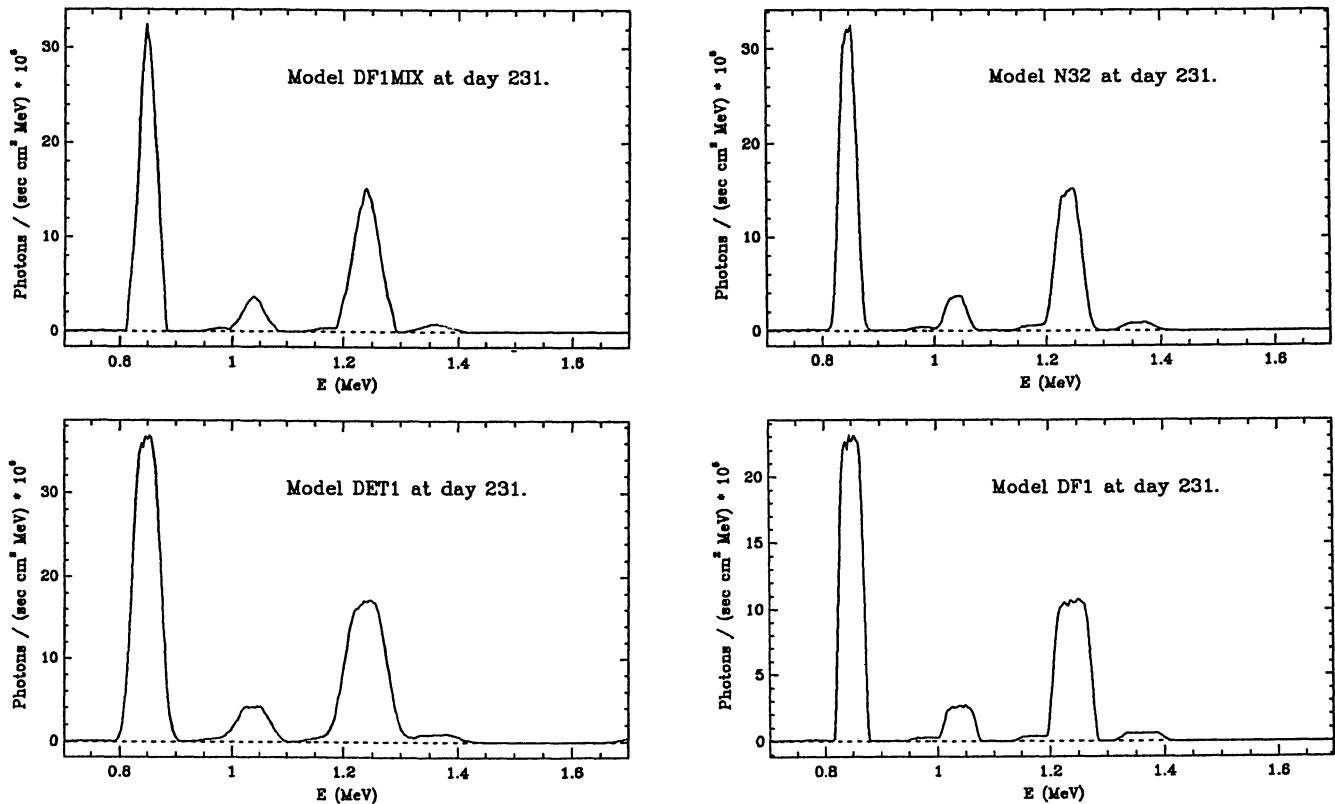


FIG. 1.— $\gamma$ -ray spectra of some models at day 231 normalized to 10 Mpc

(ii) the observing schedule is changed fast enough to catch the supernova at an early epoch (i.e., within two weeks after the explosion). Unfortunately, the latter requirement could not be fulfilled. For SN 1991T, however, observations (see Table 2 of Lichti et al. 1993) by OSSE and COMPTEL during the third (June 13–27) and eleventh (October 3–17) full-sky viewing period still allow for the determination of important constraints on models of SN Ia's (see Table 1) if these observations are combined with information coming from other wavelength bands.

Obviously, the distance is one of the critical points for the use of  $\gamma$ -ray observations unless very early measurements are available to record the change of the slope in the  $\gamma$ -ray light curve which provides a way to identify the proper explosion mechanism (see Fig. 2). Nevertheless, the distance can be determined from the optical light curves using an elaborated radiation transport scheme (Höfllich et al. 1993). Although most of the models can be excluded by the optical LCs, the LC-fits do not allow for a unique determination of the model (see Fig. 3). However, even when taking these uncertainties and those

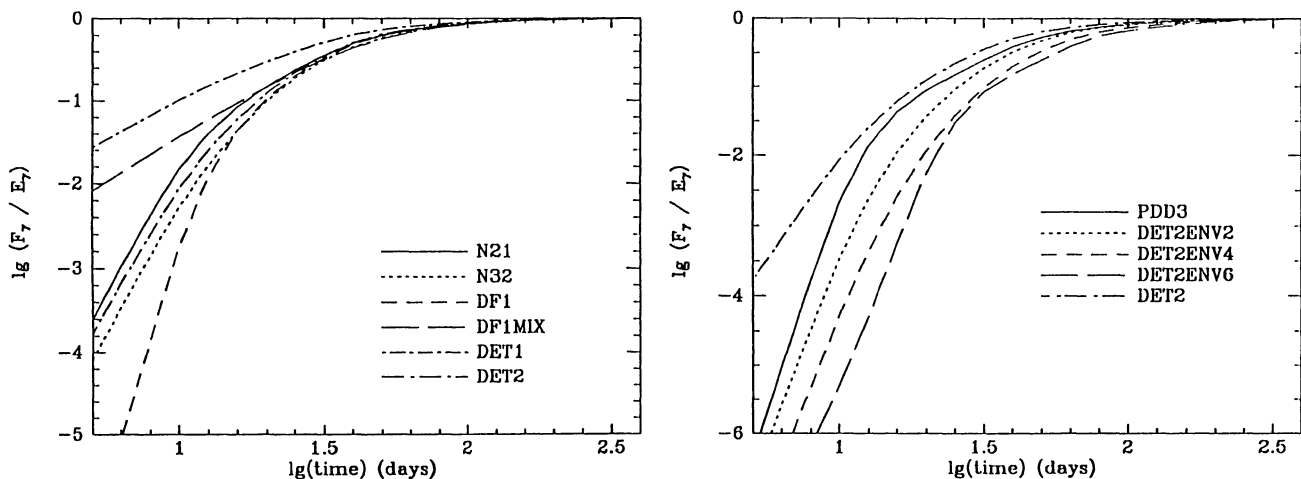


FIG. 2.—Energy radiated relative to energy being produced in form of  $\gamma$ -rays by  $^{56}\text{Ni}$  and  $^{56}\text{Co}$  decay

TABLE 1

OVERVIEW OF INVESTIGATED THEORETICAL SN Ia MODELS COVERING THE FULL RANGE OF DETONATION, DEFLAGRATION, DELAYED DETONATION, PULSATING DELAYED DETONATION, TAMPED DETONATION, AND LOW-DENSITY DETONATION MODELS

Model (1)	Mode of Explosion (2)	$M_*$ ( $M_\odot$ ) (3)	$\rho_c$ ( $10^9 \text{ g cm}^{-3}$ ) (4)	$\alpha$ (5)	$\rho_{tr}$ ( $10^7 \text{ g cm}^{-3}$ ) (6)	$E_{kin}$ ( $10^{51}$ ergs) (7)	$M_{Ni}$ ( $M_\odot$ ) (8)	$\langle v \rangle$ ( $10^8 \text{ cm s}^{-1}$ ) (9)
DET1 .....	detonation	1.4	3.5	...	...	1.75	0.92	10.1
DF1 .....	deflagration	1.4	3.5	0.30	...	1.10	0.50	8.3
DF1MIX .....	deflagration	1.4	3.5	0.30	...	1.10	0.50	8.3
N21 .....	delayed det.	1.4	3.5	0.03	5.0	1.63	0.83	9.3
N32 .....	delayed det.	1.4	3.5	0.03	2.6	1.52	0.56	9.0
PDD3 .....	pul. del. det.	1.4	2.1	0.04	2.0	1.37	0.49	9.1
CO095 .....	detonation	0.95	...	...	...	1.10	0.18	9.9
CO10 .....	detonation	1.0	...	...	...	1.22	0.32	10.1
CO11 .....	detonation	1.1	...	...	...	1.44	0.58	10.4
DET2 .....	detonation	1.2	0.04	...	...	1.52	0.63	10.3
DET2E2 .....	det. + envelope	1.2 + 0.2	0.04	...	...	1.52	0.63	9.4
DET2E4 .....	det. + envelope	1.2 + 0.4	0.04	...	...	1.52	0.63	8.7
DET2E6 .....	det. + envelope	1.2 + 0.6	0.04	...	...	1.52	0.63	8.2

NOTES.—The quantities given in cols. (3) to (9) are ( $M_*$ ) white dwarf mass; ( $\rho_c$ ) central density of the white dwarf; ( $\alpha$ ) ratio of deflagration velocity and local sound speed; ( $\rho_{tr}$ ) transition density at which the deflagration is assumed to turn into a detonation; ( $E_{kin}$ ) final kinetic energy; ( $M_{Ni}$ ) mass of synthesized  $^{56}\text{Ni}$ ; ( $\langle v \rangle$ ) average expansion velocity. In Model DF1MIX the composition was completely homogenized after burning had stopped.

TABLE 2

PHOTON COUNT RATE IN  $10^{-5}$  PHOTONS  $\text{cm}^{-2} \text{s}^{-1}$  FOR THE LINES AT 0.847 AND 1.238 MeV AT DAY 80

Line Energy (MeV)	$2\sigma$ Upper Limit	N21	N32	DF1	DF1mix	DET1	PDD3	DET2	DET2E2	DET2E6	CO095
0.847 .....	3.2	4.0	2.4	1.7	2.4	6.6	2.5	3.0	2.7	2.3	0.9
1.238 .....	2.5	2.8	1.8	1.4	1.8	4.3	1.8	2.4	2.1	1.8	0.7

NOTES.—The observed upper limit (Lichti et al. 1993) is compared to the rates from the models given in Table 1. According to the optical light curve fits, the distance of SN 1991T is taken to 12.5 Mpc.

due to interstellar reddening into account, the distance can be determined to be  $12.5 \pm 0.5$  Mpc.

Although only upper limits for the  $\gamma$ -ray line flux can be derived from the observations, they give important upper limits (Table 2). First of all, the limits clearly rule out several of

the models in accordance with the restrictions implied by the optical LCs. Second, the upper limits are consistent with models which allow for a reproduction of the optical observations and the inferred distance. Conclusively, it becomes clear that both pulsating delayed detonation (PDD3) and envelope mod-

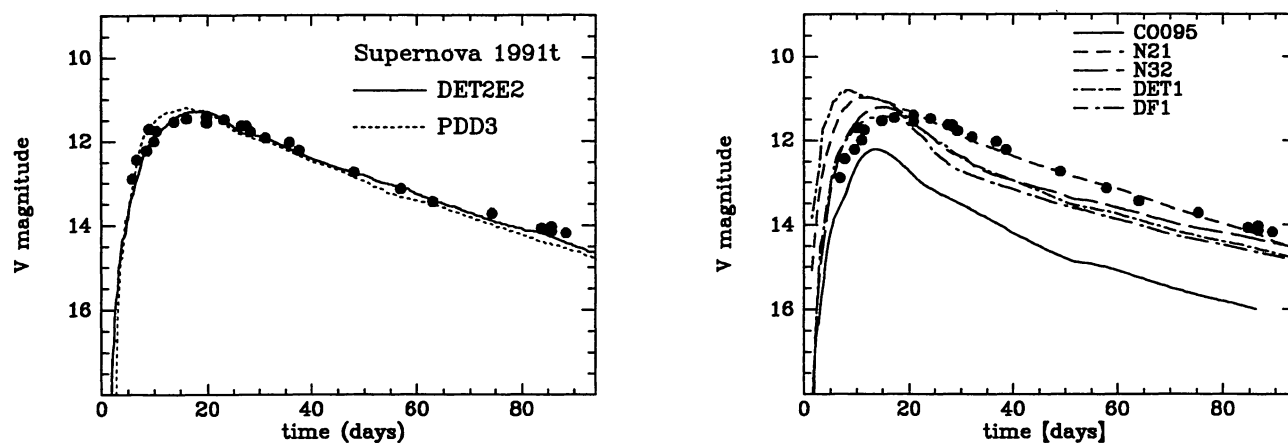


FIG. 3.—Observed visual light curve of SN 1991T in the  $V$  filter band in comparison to the calculated light curves of DET2ENV2 and PDD3 (*top*) using the derived distance of 12.5 Mpc and  $E_{B-V} = 0.08$  mag. In the second plot (*bottom*) a comparison with some of the models is given which do not allow for a reproduction of the observations.

els (DET2ENV2) can reproduce the observations of SN 1991T (Fig. 3). A slightly smaller limit for the  $\gamma$ -ray flux would clearly allow for a distinction of the two different explosion scenarios.

Finally, we want to stress the future perspectives of *CGRO* observations of SN Ia's due to the long expected live time of

*CGRO* ( $\approx 10$  yr). Statistically, about all 8 years there is a SN Ia at a distance between 4 and 9 Mpc (e.g., 4.6 Mpc for SN 1972e, 4.5 Mpc for SN 1986g, 8.4 Mpc for SN 1989b) which clearly would allow for a positive measurement of the  $\gamma$  fluxes or it would rule out all our models.

## REFERENCES

- Clayton, D. D., Colgate, S. A., & Fishman, G. J. 1969, *ApJ*, 155, 75  
Colgate, S. A., & McKee, C. 1969, *ApJ*, 157, 623  
Höfllich, P., Khokhlov, A., & Müller, E. 1993, *A&A*, 268, 570  
Höfllich, P., Müller, E., & Khokhlov, A. 1992, *A&A*, 259, 243  
Iben, I., Jr., & Tutukov, A. V. 1984, *ApJS*, 54, 335  
Khokhlov, A. 1991, *A&A*, 245, 114  
Khokhlov, A., Müller, E., & Höfllich, P. 1994, *A&A*, in press  
Lichti, G., et al. 1994, *Compton Observatory Symp.*, Washington, in press  
Müller, E., & Höfllich, P. 1993, *A&A*, submitted  
Müller, E., Höfllich, P., & Khokhlov, A. 1991, *A&A*, 249, L1  
Nomoto, K., Sugimoto, D., & Neo, S. 1976, *Ap&SS*, 39, 137  
Webbink, R. F. 1984, *ApJ*, 277, 355